Materials and Design 131 (2017) 450–459

Contents lists available at ScienceDirect

Materials and Design

journal homepage: www.elsevier.com/locate/matdes

Microstructure and mechanical properties of fibre laser welded medium manganese TRIP steel

N. Lun [a,*], D.C. Saha [a], A. Macwan [a], H. Pan [b], L. Wang [c], F. Goodwin [d], Y. Zhou [a]

[a] Department of Mechanical and Mechatronics Engineering, University of Waterloo, 200 University Avenue West, Waterloo, Ontario N2L 3G1, Canada
[b] State Key Laboratory of Development, Application Technology of Automotive Steels, Shanghai 201900, China
[c] Baosteel Research and Development Technology Center, Shanghai 201900, China
[d] International Zinc Association, Durham, NC 27713, USA

HIGHLIGHTS

- This manuscript presents fibre laser welding of novel medium manganese steel
- Dissimilar welds to high strength low alloy and dual-phase steels were achieved
- Heat affected zone softening was not observed in medium manganese steel
- Tensile joint efficiency and formability were improved by welding to dissimilar steel

GRAPHICAL ABSTRACT

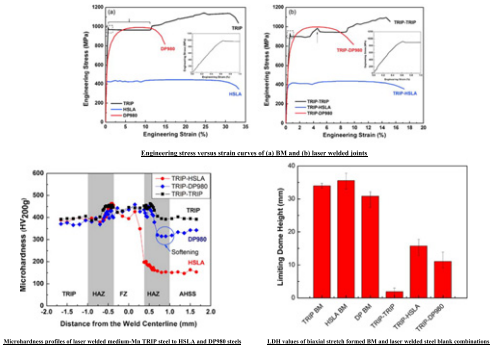

Engineering stress versus strain curves of (a) BM and (b) laser welded joints

Microhardness profiles of laser welded medium-Mn TRIP steel to HSLA and DP980 steels

LDH values of biaxial stretch formed BM and laser welded steel blank combinations

ARTICLE INFO

Article history:
Received 14 April 2017
Received in revised form 29 May 2017
Accepted 15 June 2017
Available online 16 June 2017

Keywords:
Fibre laser welds
Medium manganese TRIP steel
Microstructure
Microhardness
Tensile testing
Formability

ABSTRACT

Fibre laser welds of Fe-0.15C-10Mn-1.5Al medium-Mn transformation induced plasticity (TRIP) steel and its dissimilar combination with high strength low alloy (HSLA) and dual-phase (DP980) steel was assessed with respect to microstructure, microhardness, formability, and tensile properties. The fusion zone (FZ) of the medium-Mn TRIP steel weldment was consist of predominantly martensite with some interdendritic austenite due to high manganese concentration which stabilizes austenite. The FZ of dissimilar combinations to HSLA and DP980 steel consisted of mostly martensite. Microhardness profiles of the medium-Mn TRIP steel showed no indications of detrimental heat-affected zone (HAZ) softening despite the high base metal (BM) hardness (396 HV). Laser welds containing medium-Mn TRIP displayed similar FZ hardness values (413–438 HV). Failure of medium-Mn TRIP laser welds under uniaxial tension occurred adjacent to the FZ where localized strain accumulated. The tensile results showed consistent failure in the weaker BM of dissimilar joints at high joint efficiency (95–100%) with respect to the weaker material of the joint. Biaxial stretch formability of TRIP-TRIP similar welds was determined to be severely limited by the brittle FZ. Strain accumulation in the BM of HSLA and DP980 steel in dissimilar combinations improved formability of laser welded blanks containing medium-Mn TRIP steel.

1. Introduction

Efforts to reduce fuel consumption of passenger vehicles by reducing the curb weight have prompted increasing applications of advanced high strength steels (AHSS). First generation AHSS, such as high

* Corresponding author at: Department of Mechanical and Mechatronics Engineering, University of Waterloo, 200 University Avenue West, Waterloo, ON N2L 3G1, Canada.
E-mail address: n2lun@uwaterloo.ca (N. Lun).

http://dx.doi.org/10.1016/j.matdes.2017.06.037
0264-1275/

Table 1
Chemical compositions of steels used (wt.%).

Steel	C	Mn	Si	Al	CE_N
TRIP	0.15	10.4	0.17	1.49	N/A
HSLA	0.05	0.56	0.12	0.03	0.12
DP980	0.09	2.11	0.31	0.30	0.37

$CE_N = C + A(c) \times (Si/24 + Mn/6 + Cu/15 + Ni/60 + (Cr + Mo + Nb + V)/5 + 5B)$
$A(c) = 0.75 + 0.25 \tanh\{20 \times (C - 0.12)\}$

Table 2
Mechanical properties of steels used.

Steel	Yield strength (MPa)	Ultimate tensile strength (MPa)	Yield point elongation (%)	Total elongation (%)	UTS × El (MPa%)
TRIP	966 ± 4	1126 ± 12	9.9	32.0 ± 2.4	36,032
HSLA	428 ± 15	453 ± 19	8.6	32.3 ± 1.6	14,632
DP980	651 ± 6	998 ± 6	–	14.7 ± 0.1	14,671

strength low alloy (HSLA) and dual-phase (DP980) steels, consist of predominantly ferrite and martensite bearing microstructures and are limited in ductility as strength increases (<25,000 MPa%) [1]. Second generation AHSS consisting of high manganese (Mn) transformation induced plasticity (TRIP) and twinning induced plasticity (TWIP) steels rely on dynamic strain hardening in austenite to achieve significantly higher ductility at a higher strength (>50,000 MPa%) [1–5]. However, significant challenges in alloy cost and metallurgical effects associated with delayed hydrogen embrittlement and liquid metal embrittlement have limited their application [3,6,7]. Consequently, steels of intermediate ductility combined with high strength (>30,000 MPa%), so-called third generation steels, are looked upon as a compromise between performance and cost [8–10].

AHSS containing medium quantities (3–10 wt%) of Mn have been shown by various researchers to achieve the target mechanical properties befitting of third generation AHSS. For example, Miller observed that a Fe-5.7Mn-0.11C steel annealed at 640 °C for 1 h exhibited a UTS and uniform elongation of 1145 MPa and 30.5%, respectively [11]. Intercritical annealing of steel containing 5–7 wt% Mn at 650 °C resulted in resiliency values in excess of 30,000 MPa% [12]. Wang et al. demonstrated that intercritically annealing a cold-rolled Fe-5Mn-0.2C steel resulted in ultrafine lamellar ferrite and austenite duplex microstructure through the austenite reversion transformation annealing mechanism [13]. Lee et al. observed that annealing temperature had a significant effect on the TRIP effect in ultrafine grained Fe-6.15Mn-1.5Si-0.05C steel [14]. Furthermore, Zhang et al. produced a textured ultrafine grain steel exhibiting a UTS and uniform elongations of 1296 MPa and 29%, respectively by intercritical rolling a Fe-4.72Mn-0.2C steel [15]. In general, the literature suggests that medium-Mn steel is a viable candidate which meets the mechanical properties of a third generation AHSS.

Applications of these third generation AHSS span a wide range of automotive structural components including floor panels, pillars, and door reinforcements [16]. The adoption of these steels is dependent on the ability of joints to behave successfully after exposure to the conditions induced by common automotive welding techniques. Laser welded blanks (LWBs), in particular, have become commonplace in automotive manufacturing, enabling curb weight reduction through selective material placement in specific applications [17]. LWBs are made from two or more similar and dissimilar sheets with different thicknesses which are formed to three-dimensional automotive body parts. Therefore, a dissimilar combination of Medium-Mn TRIP to a commonly used DP980 and HSLA steels are potential applications to autobody assembly. In last decades, extensive studies have been carried out on laser beam welding of AHSS including DP, TRIP, TWIP, martensitic steel (MS), and ultra-high strength steels such as press-hardened steel (PHS) [18–21]. It has been reported that high-speed laser beam welding minimizes the HAZ softening of DP steels and improves joint efficiency [21,22]. A laser beam welding on a similar and dissimilar combination of TRIP and TWIP steel provides inhomogeneous fusion zone and formation of ε-martensite and α-martensite as a secondary phase [23,24]. Laser beam welding of Al-Si coated PHS forms a soft ferrite phase in the fusion zone due to coating mixing leading to premature failure [18–20].

Despite the apparent success in achieving the desired base metal mechanical properties, no work has been performed on the effects of welding processes on medium-Mn TRIP steel. Therefore, the focus of this study is to assess the fibre laser weldability and mechanical

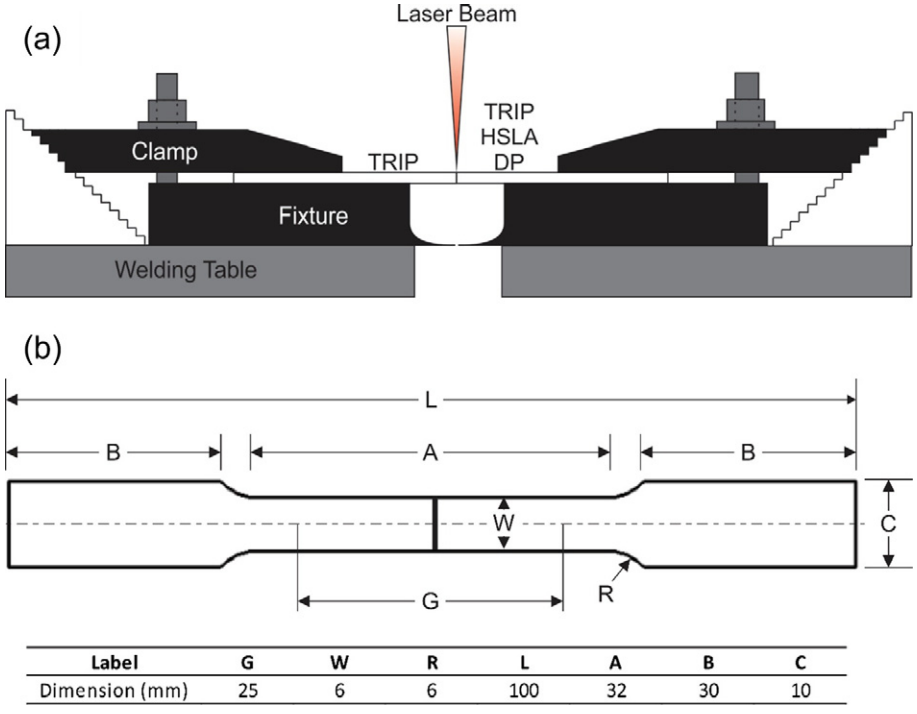

Label	G	W	R	L	A	B	C
Dimension (mm)	25	6	6	100	32	30	10

Fig. 1. Illustrative schematics of the (a) welding fixture and (b) ASTM E8 sub size tensile test specimen geometry.

properties of medium-Mn TRIP steel with respect to dissimilar combinations of HSLA and DP980 steel which are commonly used steels for automotive structural components.

2. Experimental

2.1. Material

The medium-Mn steel used in this investigation was provided by Baosteel Inc. (China) and will be henceforth referred to "medium-Mn TRIP" steel. The steel was processed by subjecting the continuously cast slab to a hot rolling and cold rolling schedule to reduce the thickness to 1.46 mm and followed by continuous intercritically annealing. The steel was passed through a galvanizing bath to produce a 50 g/m^2 galvanized coating on both sides of the sheet steel. Hot dipped galvanized HSLA and DP980 having similar thicknesses (1.2 mm) were used as the complementary steels in the laser welded blanks. The chemical compositions and mechanical properties of the steels are shown in Tables 1 and 2, respectively.

2.2. Laser welding

The edges of 100 mm × 200 mm blanks were milled and deburred to ensure a near zero-gap square butt joint when clamped in the welding fixture (Fig. 1a). Laser welding was performed in ambient air using an IPG Photonics YLS-6000 fibre laser with a core diameter of 0.6 mm and a spot size of 0.3 mm. The laser beam was delivered by a Laser Mechanisms welding head with an optical focal distance of 300 mm mounted on a Panasonic TA-1600 6-axis welding robot. A 4 × 4 Bead-on-Plate process optimization matrix was completed to select an appropriate welding parameter for the study. After narrowing down the acceptable process envelope, several trials were conducted in the butt joint configuration. It was determined that to meet the weld geometrical requirements of GMA4485, it was necessary that a defocusing study is conducted to avoid excessive concavity. From the optimization studies, it was determined that laser power of 4 kW and a linear robot movement speed of 12 m min^{-1} with a defocus distance of 5 mm above the blank surface can achieve full penetration welds with acceptable geometry. Argon assists gas was used during the welding process, with a side and back-shield channel delivery flow rate of approximately 14 LPM and 21 LPM respectively.

2.3. Microstructure characterization

Metallographic samples of laser weld cross sections were etched with a 4% Nital solution. Optical microscopy (OM) was conducted using an Olympus BX51M microscope. A ZEISS LEO1530 field-emission scanning electron microscope (FE-SEM) with a mounted energy dispersive X-ray spectrometer (EDS) was used to obtain high magnification micrographs at an accelerating voltage of 15 kV. Grain size and microstructure fractions were estimated (using image analysis software ImageJ) from 15 different micrographs taken from various regions.

2.4. Mechanical testing

Microhardness testing was performed on polished and etched weld cross sections using a Clemex-JS 2000 automated hardness tester with a 200 g load and 15 s dwell time. Indentations were sequentially distanced 2–3 times the diagonal to avoid strain field effects of the adjacent indents. The 200 mm × 200 mm laser welded blanks were machined into standard ASTM E8 sheet type subsize transverse weld tensile specimens of which the dimensions can be found below in Fig. 1(b). Three dimensional digital image correlation (DIC) by Correlated Solutions Inc. was used to observe and assess uniaxial tensile testing conducted in a Tinius Olsen H10KT tensile system at a constant cross head speed of 10 mm min^{-1}. Tensile specimens were degreased with ethanol and speckled with a randomized black-on-white pattern using spray paint. Step and subset sizes used for the DIC analysis were 19 and 7, respectively. Image capture of the DIC system was conducted at a frequency of 4 Hz. All tensile tests were repeated three times and the average values are reported.

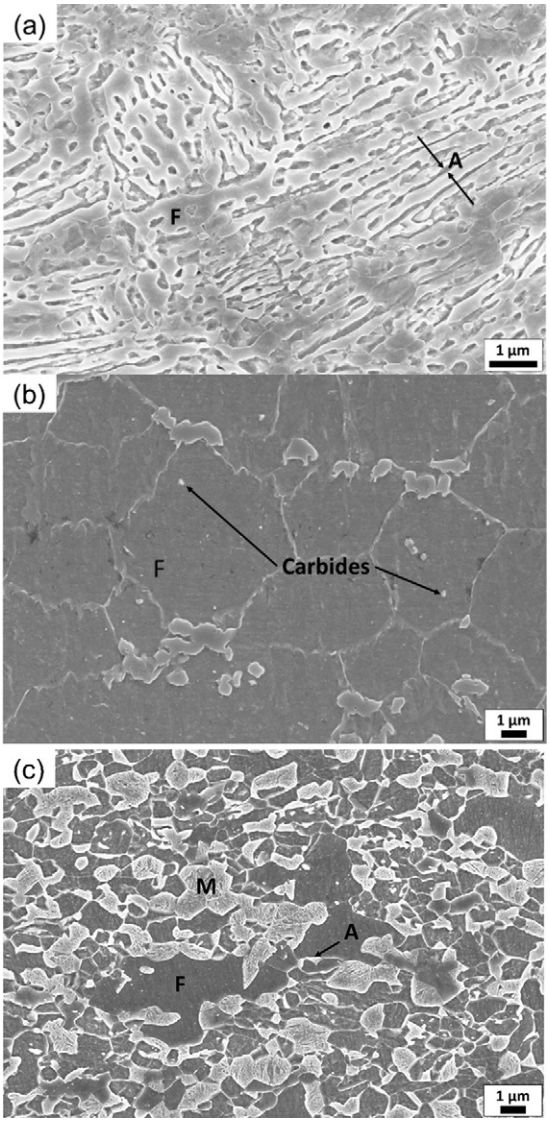

Fig. 2. SEM micrographs showing the base metal of (a) TRIP, (b) HSLA, and (c) DP980. (F: Ferrite, A: Austenite, M: Martensite).

Biaxial stretch forming was assessed through conducting Hecker's Limiting Dome Height (LDH) tests on 200 mm × 200 mm laser welded blanks. Three dimensional DIC was also performed to assess strain development during forming. Image capture of the DIC system was conducted at a frequency of 125 Hz while step and subset sizes used for the analysis were fixed at 35 and 7, respectively. Biaxial stretch forming was evaluated with the MTS 866 hydraulic press with a hemispherical punch having a diameter of 101.6 mm with a circular draw bead diameter of 132 mm. A clamping force of 650 kN was exerted on the blank to prevent draw in and the punch was advanced upwards at a rate of 0.2 mm/s until a significant load drop occurred on the hydraulic analog readout. All LDH results reported were averaged across five trials.

3. Results and discussion

3.1. Microstructure

The BM microstructures of the medium-Mn TRIP, HSLA, and DP980 steels are illustrated by the micrographs in Fig. 2. The medium-Mn TRIP steel microstructure comprised a mixture of the ultrafine lamellar structure of austenite embedded in a ferrite matrix (Fig. 2(a)). The

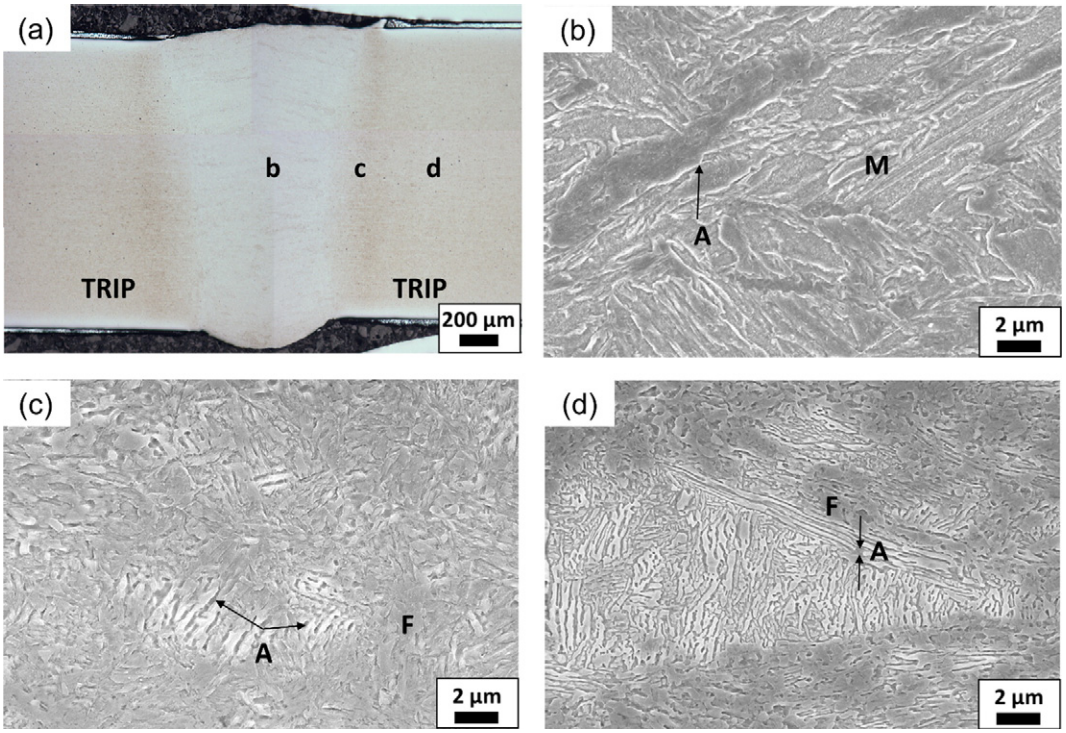

Fig. 3. SEM micrographs of TRIP-TRIP laser weld cross section; (a) full weld profile, (b) FZ, (c) HAZ, (d) TRIP BM. (A: austenite, F: ferrite, M: martensite).

average width of the austenite laths ranged from approximately 100–400 nm. Denser lamellar colonies were observed dispersed throughout the steel and exhibiting narrower lath widths. The microstructure was consistent with findings from literature which reported that intercritically annealed medium Mn steels are prone to developing lamellar duplex microstructures of austenite and ferrite [1,13,15,25–27]. The microstructure of the HSLA steel was found to consist of finely dispersed carbides in ferrite grains with a measured average grain size of 7.15 ± 0.73 μm (Fig. 2(b)). The DP980 steel contained martensite islands embedded in a ferritic matrix with a small fraction of retained austenite (Fig. 2(c)).

Fig. 3(a) shows the cross-section overview of a TRIP-TRIP weld. The FZ microstructure as illustrated in Fig. 3(b) consisted primarily of lath martensite, however, the original dendritic solidification structure decorated by austenite was still visible. Darker austenitic regions between dendrite cores suggested the occurrence of C and Mn micro-segregation phenomena during solidification, which has been observed in welds of high Mn content AHSS [24,28,29]. The enrichment of the interdendritic regions can suppress the formation of martensite and thereby possibly result in retained austenite [30]. However, unlike high Mn AHSS, the Mn content in medium-Mn TRIP steels appears to be insufficient to produce a fully austenitic FZ microstructure after laser welding. The average concentration of Mn in the FZ of the TRIP-TRIP weld compared to the TRIP BM was measured by EDS to be approximately 10.4 ± 0.1 wt% and 10.2 ± 0.2 wt% respectively. Compared to high-Mn steels, the amount of Mn evaporation during fibre laser welding in med-Mn steel appears to be negligible [23]. In Fig. 3(c), the microstructure of the HAZ consisted of a dense network-like structure of ferrite and austenite compared to the distinct lamellar structure observed in the BM (Fig. 3(d)). The microstructures observed across the HAZ were not distinct enough to qualitatively distinguish between specific temperature zones.

Fig. 4 illustrates the different regions in the TRIP-HSLA laser welded specimens. The FZ of the TRIP-HSLA laser weld (Fig. 4(b)) appeared to consist primarily of martensite formed upon rapid cooling of the weld pool. Austenite in the FZ could not be determined by qualitative observations of the SEM micrographs. This can be attributed to the FZ mixing between the low Mn content in the HSLA and the medium-Mn TRIP steel. The supercritical region in the HSLA steel (Fig. 4(c)) adjacent to the FZ consisted of martensite, and the intercritical HAZ of the HSLA side (Fig. 4(d)) revealed nucleation of martensite between ferrite grains. Both are typical HAZ microstructures observed in laser welded HSLA steel [21].

Fig. 5 shows the cross section of the TRIP-DP980 laser weld along with the microstructural evolution across the respective regions. The FZ displayed mainly autotempered martensite, while the presence of austenite was indiscernible (Fig. 5(b)). Similar to the TRIP-HSLA welds, the dilution of the Mn in the FZ contributed to reducing austenite stability, effectively preventing the presence of retained austenite in the FZ. The micrographs of the TRIP-DP980 welds suggested that the DP980 side consisted of typical microstructures observed in laser welded DP steel [21,31]. The supercritical DP980 HAZ (Fig. 5(c)) contained well defined martensite blocks with large high-angle grain boundaries delineating the prior-austenite grain boundaries. The intercritical HAZ (Fig. 5(d)) contained a continuous network of newly transformed martensite and ferrite. The SCHAZ exhibited pre-existing martensite that was tempered by exposure to temperature slightly below the Ac_1 line (Fig. 5(e)) [32].

3.2. Microhardness

Fig. 6 shows the microhardness profiles on cross sections of TRIP-TRIP, TRIP-HSLA and TRIP-DP980 welds. The microhardness of the TRIP BM was determined to be 396 ± 10 HV. Although most the microstructure consisted of ferrite and austenite (Fig. 2(a)), the ultrafine lamellar structure of austenite resulted in a high BM hardness value. The TRIP-TRIP microhardness profile revealed no HAZ softening, which can be attributed to the lack of martensite in the BM since it was reported previously that HAZ softening is a function of both martensite content in BM and heat input [31]. The supercritical HAZ of the welded joint exhibited the highest hardness values of about 463 HV which can be attributed to the formation of martensite at the rapid

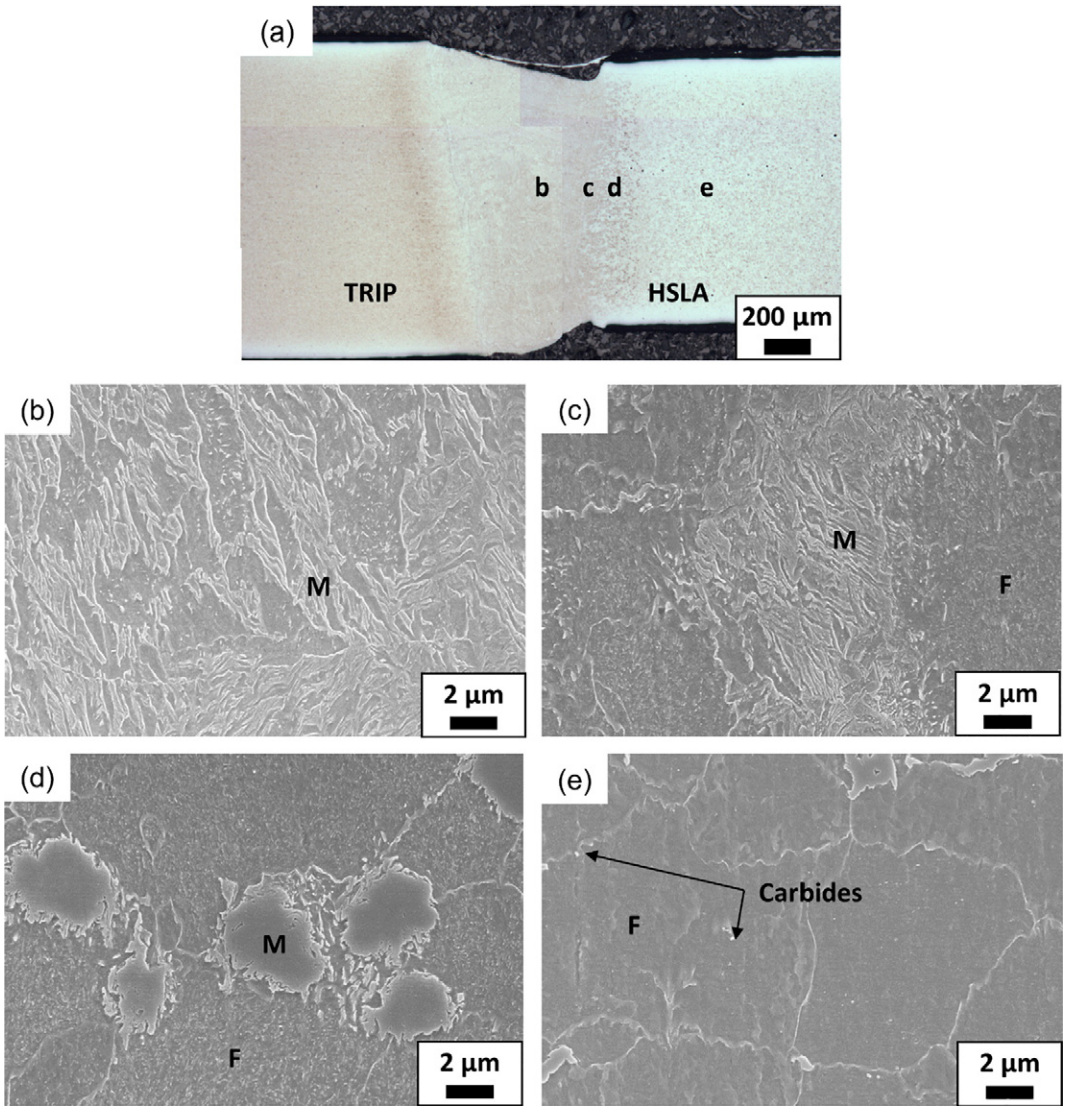

Fig. 4. Micrographs of TRIP-HSLA laser weld cross section; (a) full weld profile, (b) FZ, (c) supercritical HAZ, (d) intercritical HAZ, and (e) HSLA BM (F: Ferrite, M: Martensite).

cooling rates experienced by the steel adjacent to the FZ. The effects of rapid local thermal cycles on the microstructural stability of medium-Mn TRIP steel are not fully understood in literature. However, the ultra-fine lamellar duplex microstructure of austenite and ferrite appears to be sufficiently stable to avoid significant grain coarsening observed in high-Mn steels despite the during short exposure time at elevated temperatures present during laser welding [28]. The FZ of the weld exhibited an average hardness of 421 ± 16 HV, apparently slightly higher than the BM hardness (396 ± 10 HV), which is attributed to the presence of martensite in the FZ.

The HSLA steel (Fig. 2(b)) was significantly softer (155 ± 9 HV) due to large polygonal ferrite grains which offer less resistance to the applied load during hardness testing. The hardness profile of the HSLA steel gradually increased when approaching the FZ of the weld, which can be attributed to the nucleation of martensite at the ferrite grain boundaries caused by the rapid thermal cycle during laser welding [21,33]. The FZ of the TRIP-HSLA weld had an average hardness of 413 ± 13 HV. The hardness of the FZ was lower than that of the TRIP-TRIP FZ which may be a result of the reduced carbon content from mixing of the two different steel chemistries.

The microhardness of the DP980 steel BM was measured to be 343 ± 8 HV; a slight reduction in sub-critical (SCHAZ) hardness (~315 HV) on the DP980 side of the joint was observed which is due to the tempering of pre-existing martensite [21,31]. The autotempered martensitic FZ of the TRIP-DP980 weld had an average hardness of 438 ± 11 HV, which is higher than the FZ of the TRIP-TRIP weld where the microstructure was a combination of martensite and austenite phase.

3.3. Tensile properties

Fig. 7(a) presents the representative BM engineering stress versus strain curves of TRIP, HSLA, and DP980 steel. The TRIP steel exhibited upper and lower yield strengths (YS) of 995 MPa and 966 MPa, respectively (inset of Fig. 7(a)). A large yield point elongation of approximately 10% was detected as a result of Lüders band formation [9,34–36]. This behavior is consistent with the tensile curves in the literature of medium-Mn steels, which suggest a pronounced TRIP effect [1,11,15,26,37]. Unlike traditional first generation TRIP steels where the TRIP effect is stress induced, the transformation induced plasticity in medium-Mn steels is largely influenced by a local plastic strain front initiated by the movement of Lüders bands [35]. Lee et al. studied the velocity at which the Lüders bands travel across the gauge length of medium-Mn TRIP steels and determined that the subsequent

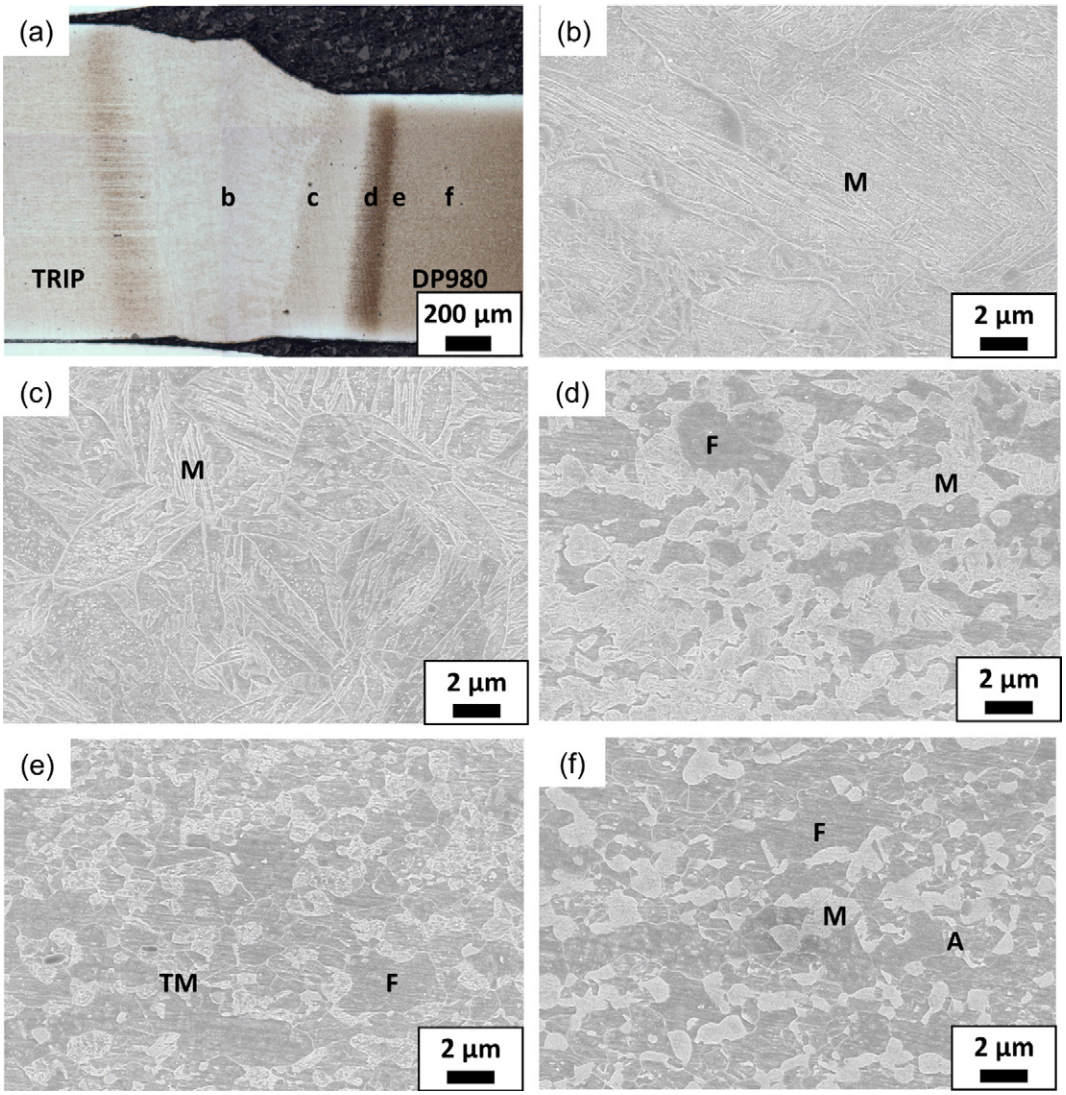

Fig. 5. Micrograph of TRIP-DP980 laser weld cross section. (a) full weld profile, (b) FZ, and HAZ on the DP980 side showing (c) supercritical HAZ, (d) ICHAZ, (e) SCHAZ, (f) DP980 BM. (A: Austenite, F: Ferrite, M: Martensite, TM: Tempered martensite).

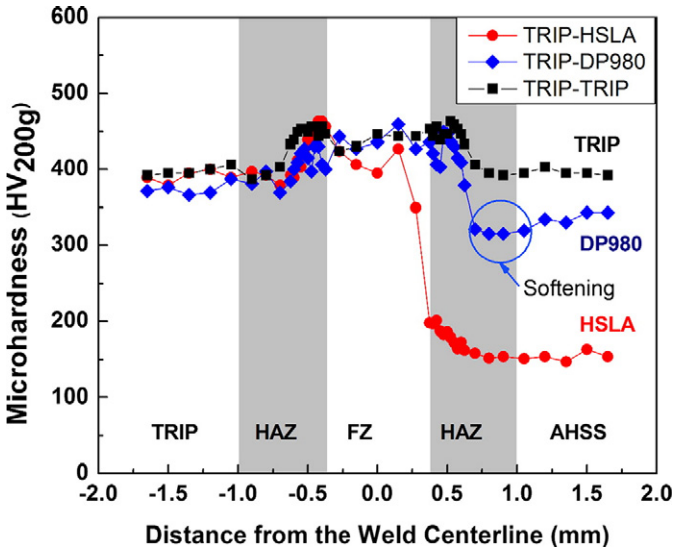

Fig. 6. Microhardness profiles of laser welded medium-Mn TRIP steel to HSLA and DP980 steels.

movement results in the significant strain-dependant transformation of the austenite into ε-martensite [38]. The ultimate tensile strength (UTS) and total uniform elongation of the TRIP steel were determined to be 1126 MPa and 32%, respectively. Therefore, the tensile strength and ductility product were calculated to be 36,032 MPa% which aligns with the target mechanical properties for a third generation AHSS [1]. The HSLA steel exhibited lower YS, UTS, and elongation of 428 MPa, 453 MPa, and 32.3%, respectively. The DP980 steel was determined to have a YS, UTS, and elongation of 651 MPa, 998 MPa, and 14.7%, respectively.

The engineering stress-strain curves of laser welded blanks consisting of TRIP-TRIP, TRIP-HSLA and TRIP-DP980 are presented in Fig. 7(b) and the mechanical properties are summarized in Table 3. From the tensile tests, it was observed that the TRIP-TRIP weld had a YS, UTS, and elongation of 897 MPa, 1091 MPa, and 16.2%, respectively. The joint efficiency of the weld, determined as the ratio of the UTS of the welded joint to that of the medium-Mn TRIP steel, was 95.9%. Comparatively, the tensile strength of the joint appeared to achieve desirable values; however, the total elongation was significantly lower than the BM. The TRIP-TRIP weld showed a significant decrease in ductility as fracture occurred after the yield point elongation. It was observed that the beginning of the yield point elongation marks the entrance of the Lüders band front into the reduced section of the specimen. As it travels

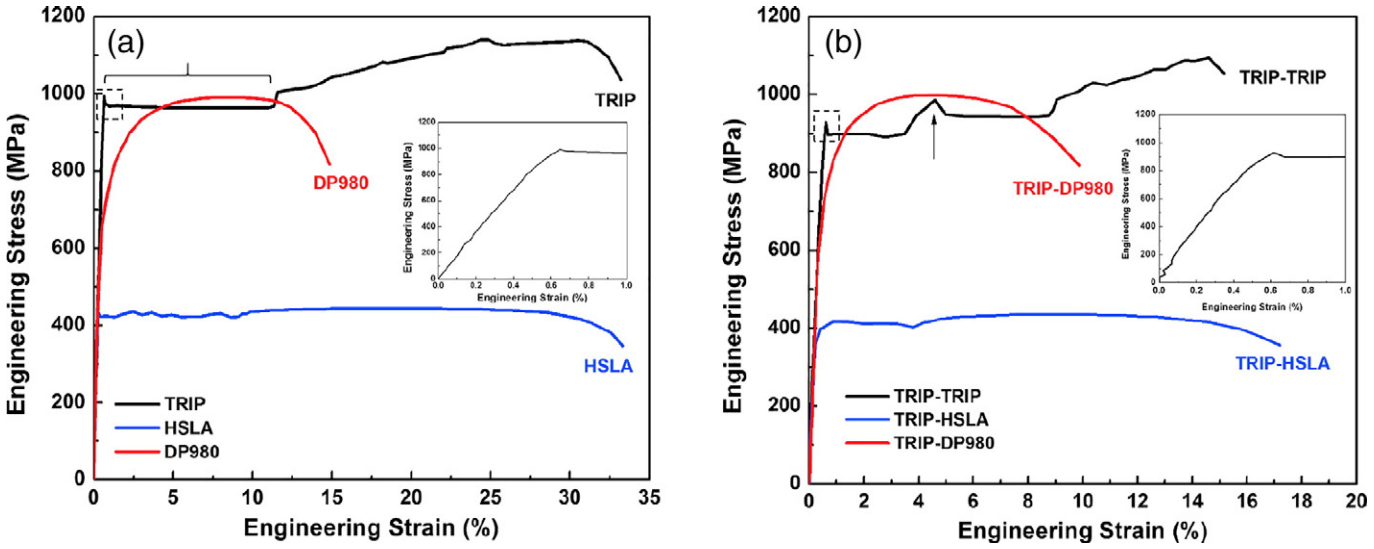

Fig. 7. Representative engineering stress versus strain curves of (a) BM and (b) laser welded joints tested at a constant cross head travel speed of 10 mm min^{-1}. The bracket in (a) delineates the yield point elongation region of the TRIP BM whereas the arrow in (b) indicates the secondary yield point that occurs in the TRIP-TRIP laser welded specimens.

across the gauge length, the band front encounters the FZ, which mainly consists of martensite, thus effectively becomes an impediment to the plastic deformation front traveling across the BM. As a result, the engineering stress increases to a secondary upper yield point (marked with a vertical arrow in Fig. 7(b)). Before fracture occurs, the Lüders band front initiates on the other side of the weld bead and continues towards the other end of the gauge length. This phenomena result in the reduction in gauge width across the entire gauge length of the tensile specimen. After the Lüders band exits the gauge length, subsequent work hardening occurs. Therefore, the secondary yield point phenomenon in the engineering stress-strain curve can be attributed to the effect of the non-uniform microstructure imposed by the laser weld, which causes significant strain concentration on either side of the weld bead resulting in fracture (Fig. 8) as will be explained in a later section.

The tensile curve of the TRIP-HSLA welded specimen behaved similarly to that of the HSLA steel BM as the welded joint failed in the HSLA side. Nominal YS, UTS, and elongations achieved by the TRIP-HSLA welded specimen were determined to be 414 MPa, 442 MPa, and 17.1%, respectively. Provided that the YS and the UTS of the welded joint were similar to that of the weaker HSLA steel, it is reasonable to suggest that most of the deformation occurred in the HSLA steel BM, which is confirmed by a final fracture in the HSLA steel BM (Fig. 8). Given that the YS of the medium-Mn TRIP steel is significantly larger than the YS of the HSLA, the HSLA steel begins to plastically deform before the TRIP finishes elastically deforming. Therefore, the weld becomes an anchor point and effectively reduces the gauge length of the specimen, resulting in an overall decrease in perceived elongation. The laser welded TRIP-HSLA specimen achieved a joint efficiency of 97.9% with respect to the HSLA steel.

The tensile response of the TRIP-DP980 welded specimen indicated deformation behavior akin to the BM of DP980 due to the higher yield strength of the TRIP BM. The YS, UTS, and elongations achieved by the TRIP-DP980 welded specimen were determined to be 602 MPa, 1005 MPa, and 9.3%, respectively. The joint efficiency was determined to be about 100% when considering the weaker DP980 BM as the basis for comparison. The reduction in ductility of the welded specimen can be attributed to the fact that deformation occurs in the DP980 prior to the onset of yielding in the medium-Mn TRIP steel. Despite the small reduction in hardness in the SCHAZ of the DP980 steel as shown previously, the softened zone was not significant enough to reduce the mechanical properties and induce an elevated stress concentration region. Ultimately, fracture of the welded specimen occurred in the BM of the DP980 steel (Fig. 8).

Fig. 9 shows the development of local axial strain along the gauge length of the welded specimens at various stages of deformation during tensile loading. Fig. 9(a) represents the plastic strain development in TRIP-TRIP welded specimens. The shape of the strain profile was clearly bimodal, showing evidence of a decrease in strain in the FZ region. Fig. 9(b) and (c) illustrate the strain development in the TRIP-HSLA and TRIP-DP980 laser welded specimens, respectively. In contrast to the TRIP-TRIP specimen, the strain concentration occurred only on the weaker materials i.e., at the HSLA side for TRIP-HSLA joint and DP980

Table 3
Mechanical properties of laser welded joints.

Specimen	Yield strength (MPa)	Ultimate tensile strength (MPa)	Elongation (%)	Joint efficiency (%)	UTS × El (MPa%)
TRIP-TRIP	897 ± 3	1091 ± 1	16.2 ± 0.6	95.9	17,722
TRIP-HSLA	414 ± 8	442 ± 6	17.1 ± 0.3	97.6	7560
TRIP-DP980	602 ± 6	1005 ± 9	9.3 ± 0.3	100.1	9310

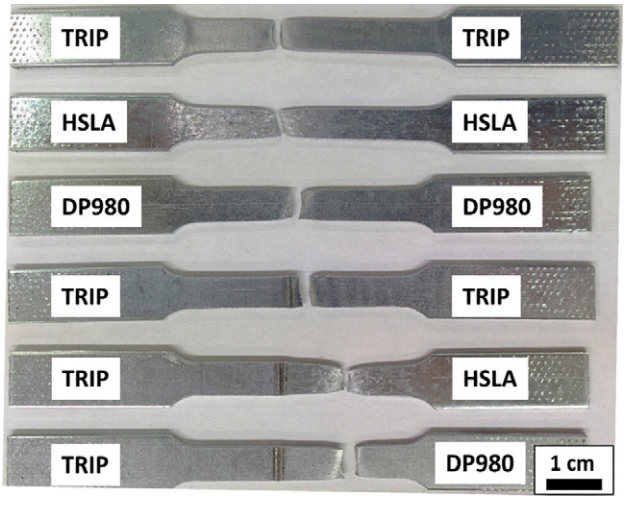

Fig. 8. Typical tensile failure locations for BM and laser welded joints.

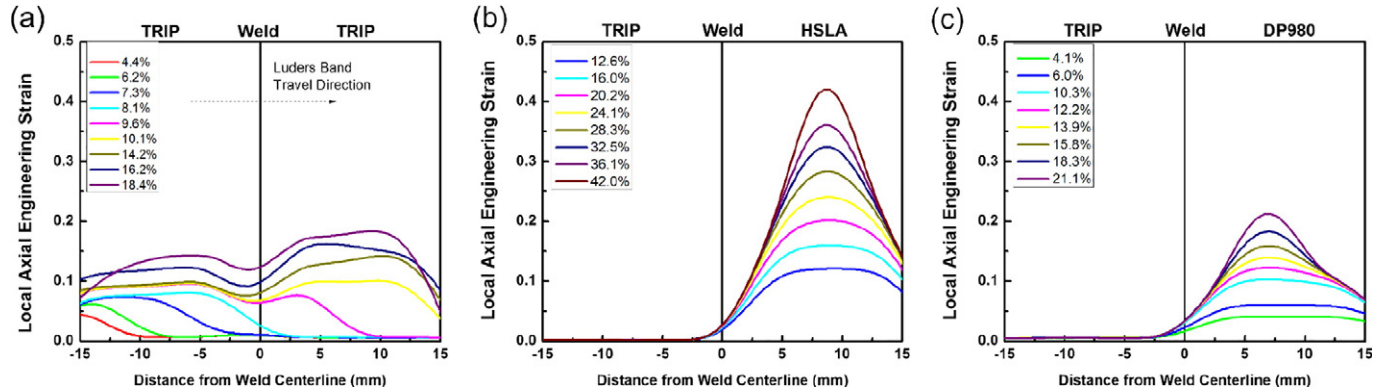

Fig. 9. Axial strain development along the gauge length of the tensile specimen at various time steps during uniaxial tensile testing of the (a) TRIP-TRIP, (b) TRIP-HSLA and (c) TRIP-DP980 laser welded specimens.

side for the TRIP-DP980 joint. As discussed earlier, the degree of HAZ softening in the TRIP-DP980 weld was small and had a negligible effect on the weld performance. Fig. 9(c), vividly shows that the majority of the strain was concentrated approximately 7 mm away from the weld centerline, whereas SCHAZ is about 0.6 mm away from the FZ, confirming that HAZ softening is not detrimental for this particular steel chemistry combination.

Fig. 10 illustrates the progression of local axial engineering strain across the gauge length of the TRIP-TRIP laser welded tensile specimen. The strain profile clearly shows that as the Lüders band propagates from one end of the gauge length, it raises the local strain by approximately 7% (position 2). Ryu et al. [35] reported that the localized deformation front is responsible for austenite to martensite strain induced transformation for a Fe-0.055C-5.6Mn-0.49Si-2.2Al wt% alloy steel. As a result, a large axial strain differential is accompanied by cross section area reduction where the Lüders band has passed through. However, as the front reaches the FZ, it is arrested by the hard, martensitic microstructure present in the weld bead (position 3). This results in a local decrease in axial engineering strain as the martensite does not plastically deform to the same degree as the BM microstructure. Therefore, the secondary yield point phenomenon noticed in Fig. 7(b) is a direct result of the Lüders band front impediment by the laser weld FZ. If the specimens do not fail in the FZ, a secondary Lüders band front initiates on the other side of the weld (position 4). The secondary band front results in a bimodal strain distribution on either side of the weld. When the Lüders band exits the other end of the gauge length (position 5), plastic strain begins to accumulate in the region adjacent to the FZ due to the large difference in cross section area. Consequently, the large difference in local strain between the hard FZ and the softer BM results in the initiation of premature fracture under tensile loading (position 6).

3.4. Formability

Figs. 11 and 12 illustrate the strain profiles and LDH values obtained by biaxial stretch forming the BM and laser welded blanks. Given the monolithic nature of the BM steels, the strain profiles are largely parabolic in nature with the majority of the strain localized near the center of the punch. According to Fig. 11(a), the medium-Mn TRIP has a wider and more distributed strain profile compared to both the HSLA (Fig. 11(b)) and DP980 (Fig. 11(c)) steels. The HSLA steel appears to favor multiple strain localization areas whereas the strain in the DP980 steel is concentrated at the center. The LDH values obtained for the TRIP, HSLA, and DP980 steels were 34.0 ± 0.6 mm, 35.6 ± 1.6 mm, and 30.8 ± 1.8 mm, respectively.

Fig. 11(d) illustrates the strain profile of the TRIP-TRIP laser welded blank. The blank immediately fractured along the FZ centerline upon punch contact at a maximum LDH value of 1.9 ± 1.1 mm, suggesting that laser welds of the medium-Mn TRIP steel are extremely brittle

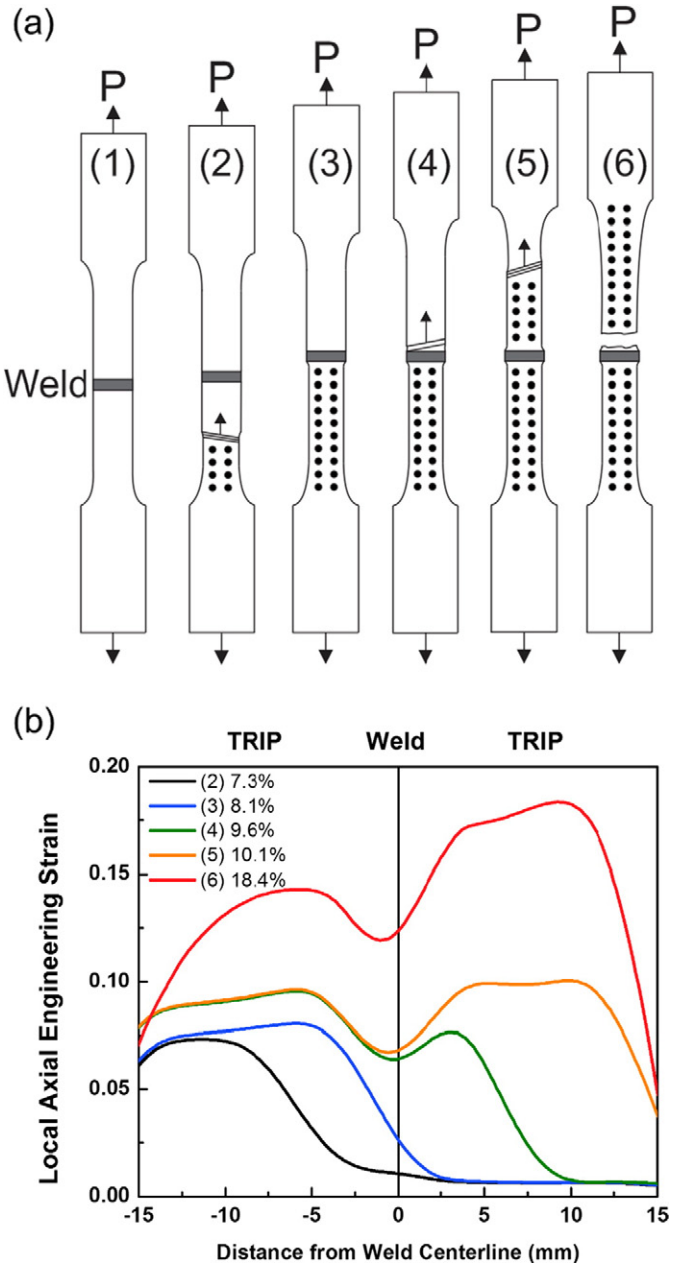

Fig. 10. Schematic illustration of the (a) TRIP-TRIP laser welded tensile specimen loaded under uniaxial tensile strain and the (b) corresponding local axial engineering strain profiles present at various stages.

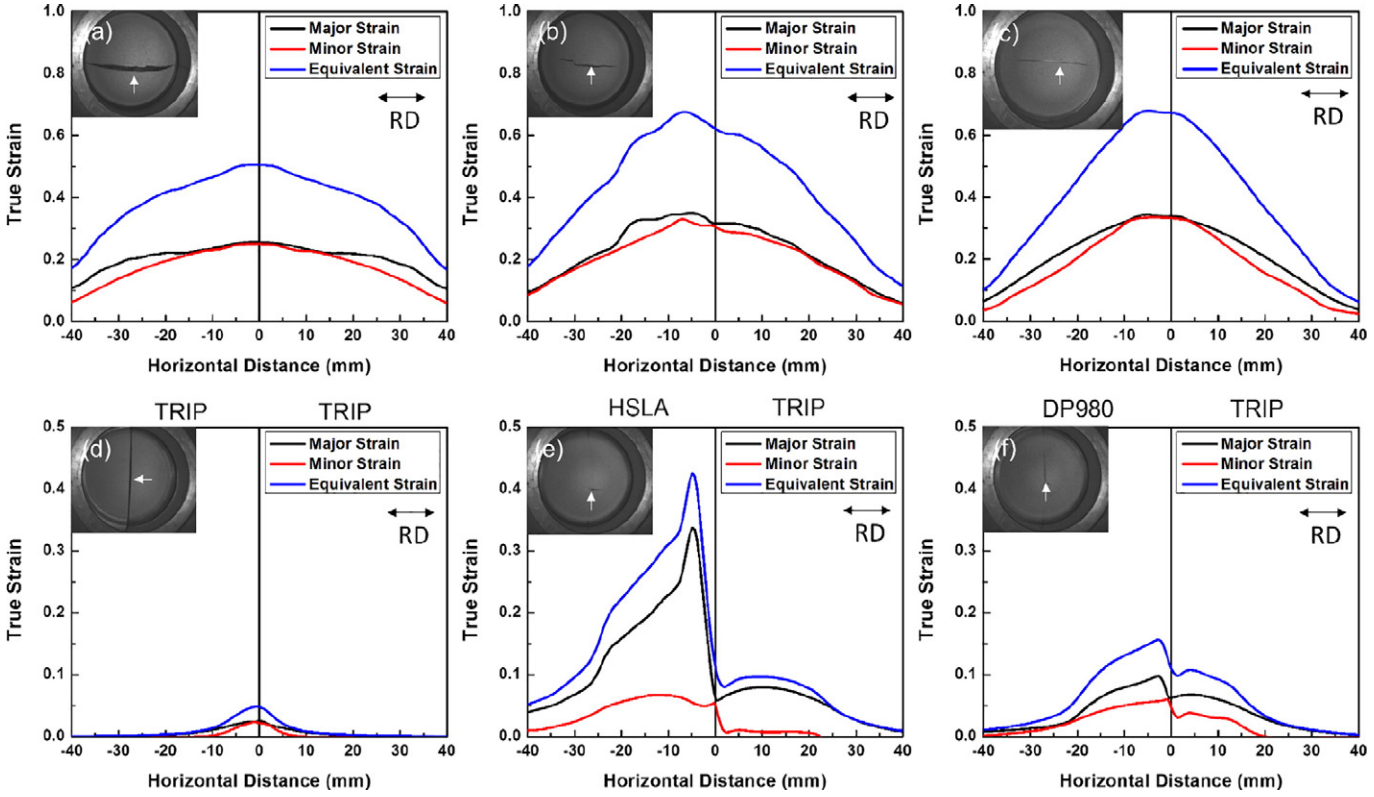

Fig. 11. Strain profiles parallel to the rolling direction of base metal and laser welded blanks under biaxial stretch forming. Top row (BM): (a) TRIP, (b) HSLA, (c) DP980; bottom row (laser welded blanks): (d) TRIP-TRIP, (e) TRIP-HSLA, (f) TRIP-DP980. (White arrow in the inset indicates initial fracture location).

when subjected to out of plane loading. The TRIP-HSLA specimen (Fig. 11(e)) achieved an average LDH value of 15.7 ± 1.7 mm. The strain profile transverse to the weld line indicated a disproportionate plastic strain occurring approximately 5 mm towards the HSLA side of the specimen. Fracture of the specimen was first observed to occur transverse to the weld line approximately 15 mm from the punch center. Fig. 11(f) shows the representative strain profile obtained by the TRIP-DP980 specimen. The maximum true strain achieved by the TRIP-DP980 combination was lower than the TRIP-HSLA specimen but higher than the TRIP-TRIP specimen. Comparatively, the strain distribution ratio between the DP980 and medium-Mn TRIP sides of the blank was significantly closer than the TRIP-HSLA specimens. This can be attributed to the smaller difference in YS of the two base metals. The LDH value achieved by the TRIP-DP980 combination was observed to be 11.1 ± 1.7 mm. Fracture of the TRIP-DP980 laser welded blank generally initiated transverse to the weld line and eventually progressed to a crack parallel to the weld. This suggests that the effects of HAZ softening were still present during out-of-plane deformation and must be taken into consideration when forming laser welded blanks using DP980 steel.

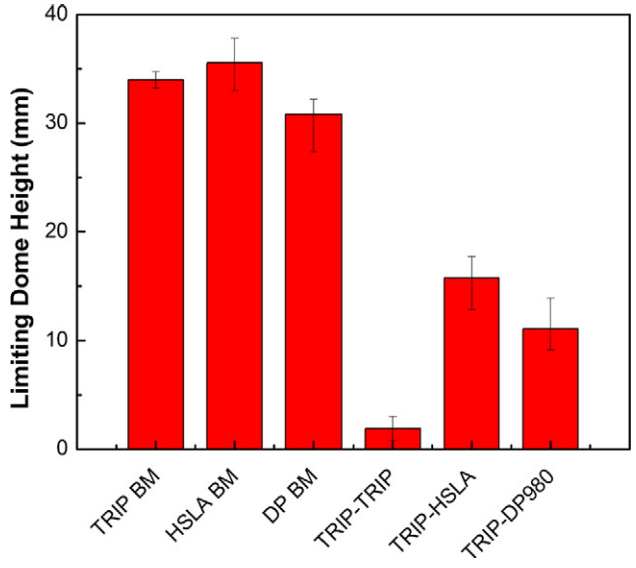

Fig. 12. LDH values of biaxial stretch formed BM and laser welded steel blank combinations.

4. Conclusions

Medium-Mn TRIP steel, HSLA steel and DP980 steel and their dissimilar laser welded combinations were investigated in relation to their microstructure, hardness and mechanical properties. The following conclusions were derived from this study:

1. The FZ of the laser welded TRIP-TRIP specimens consisted primarily of martensite with a small amount of austenite between dendrite cores. Dissimilar welds with HSLA and DP980 produced primarily martensitic FZ with similar hardness. No HAZ softening in the medium-Mn TRIP steel was observed due to remarkably high temperature stable microstructure and a lack of pre-existing martensite in the BM.
2. The laser welded TRIP-TRIP joints achieved approximately 96% joint efficiency with respect to the BM. TRIP-TRIP laser welded specimens were observed to exhibit a secondary yield point due to the impediment of the strain-induced transformation by the martensitic FZ microstructure. Dissimilar welds failed in BM of the DP980 and HSLA steel due to yielding in the weaker substrate material.

3. Formability of TRIP-TRIP laser welded blanks was severely limited by the brittle nature of the fusion zone when subjected to biaxial stretch loading conditions. Forming ductility of TRIP-HSLA and TRIP-DP980 steels demonstrated significant improvement by shifting the stress localization towards the weaker steel.

Acknowledgements

Authors would like to acknowledge the International Zinc Association in Durham, NC, USA and the National Science and Engineering Research Council (NSERC) of Canada for providing financial support. Authors are thankful to Dr. Michael Worswick for granting access to forming equipment.

References

[1] Y.-K. Lee, J. Han, Current opinion in medium manganese steel, Mater. Sci. Technol. 31 (2015) 843–856.
[2] L. Chen, Y. Zhao, X. Qin, Some aspects of high manganese twinning-induced plasticity (TWIP) steel, a review, Acta Metall. Sin. (English Lett.) 26 (2013) 1–15.
[3] B.C. De Cooman, O. Kwon, K.-G. Chin, State-of-the-knowledge on TWIP steel, Mater. Sci. Technol. 28 (2012) 513–527.
[4] B.C. De Cooman, K. Chin, J. Kim, High Mn TWIP steels for automotive applications, New Trends Dev. Automot. Syst. Eng 2011, pp. 1001–1128.
[5] H. Kim, D.-W. Suh, N.J. Kim, Fe–Al–Mn–C lightweight structural alloys: a review on the microstructures and mechanical properties, Sci. Technol. Adv. Mater. 14 (2013) 14205.
[6] J.H. Ryu, S.K. Kim, C.S. Lee, D.-W. Suh, H.K.D.H. Bhadeshia, Effect of aluminium on hydrogen-induced fracture behaviour in austenitic Fe-Mn-C steel, Proc. R. Soc. A Math. Phys. Eng. Sci. 469 (2012) 20120458.
[7] M. Koyama, E. Akiyama, T. Sawaguchi, D. Raabe, K. Tsuzaki, Hydrogen-induced cracking at grain and twin boundaries in an Fe-Mn-C austenitic steel, Scr. Mater. 66 (2012) 459–462.
[8] H.L. Yi, K.Y. Lee, H.K.D.H. Bhadeshia, Extraordinary ductility in Al-bearing delta-TRIP steel, Proc. R. Soc. A Math. Phys. Eng. Sci. 467 (2011) 234–243.
[9] D.W. Suh, J.H. Ryu, M.S. Joo, H.S. Yang, K. Lee, H.K.D.H. Bhadeshia, Medium-alloy manganese-rich transformation-induced plasticity steels, Metall. Mater. Trans. A Phys. Metall. Mater. Sci. 44 (2013) 286–293.
[10] H. Aydin, E. Essadiqi, I.H. Jung, S. Yue, Development of 3rd generation AHSS with medium Mn content alloying compositions, Mater. Sci. Eng. A 564 (2013) 501–508.
[11] R.L. Miller, Ultrafine-grained microstructures and mechanical properties of alloy steels, Metall. Trans. A. 3 (1972) 905–912.
[12] M.J. Merwin, Hot- and cold-rolled low-carbon managaese TRIP steels, Proc. SAE Intl. World Congr. Exhib, 2007 (pp. 2007-01–0336).
[13] C. Wang, J. Shi, C.Y. Wang, W.J. Hui, M.Q. Wang, H. Dong, W.Q. Cao, Development of ultrafine lamellar ferrite and austenite duplex structure in 0.2C5Mn steel during ART-annealing, ISIJ Int. 51 (2011) 651–656.
[14] S. Lee, S.J. Lee, S. Santhosh Kumar, K. Lee, B.C. De Cooman, Localized deformation in multiphase, ultra-fine-grained 6 Pct Mn transformation-induced plasticity steel, Metall. Mater. Trans. A Phys. Metall. Mater. Sci 2011, pp. 3638–3651.
[15] R. Zhang, W.Q. Cao, Z.J. Peng, J. Shi, H. Dong, C.X. Huang, Intercritical rolling induced ultrafine microstructure and excellent mechanical properties of the medium-Mn steel, Mater. Sci. Eng. A 583 (2013) 84–88.
[16] Y. Ma, Medium-manganese steels processed by austenite-reverted-transformation annealing for automotive applications, Mater. Sci. Technol. (2017) 1–15.
[17] M. Merklein, M. Johannes, M. Lechner, A. Kuppert, A review on tailored blanks - production, applications and evaluation, J. Mater. Process. Technol. 214 (2014) 151–164.
[18] D.C. Saha, E. Biro, A.P. Gerlich, N.Y. Zhou, Fusion zone microstructure evolution of fiber laser welded press-hardened steels, Scr. Mater. 121 (2016) 18–22.
[19] D.C. Saha, E. Biro, A.P. Gerlich, N.Y. Zhou, Fiber laser welding of Al-Si-coated press-hardened steel, Weld. J. 95 (2016) (147–s–156–s).
[20] C. Kim, M.J. Kang, Y.D. Park, Laser welding of Al-Si coated hot stamping steel, Procedia Eng 2011, pp. 2226–2231.
[21] D.C. Saha, D. Westerbaan, S.S. Nayak, E. Biro, A.P. Gerlich, Y. Zhou, Microstructure-properties correlation in fiber laser welding of dual-phase and HSLA steels, Mater. Sci. Eng. A 607 (2014) 445–453.
[22] D.C. Saha, E. Biro, A.P. Gerlich, Y. Zhou, Effects of tempering mode on the structural changes of martensite, Mater. Sci. Eng. A 673 (2016) 467–475.
[23] L. Mújica Roncery, S. Weber, W. Theisen, Welding of twinning-induced plasticity steels, Scr. Mater. 66 (2012) 997–1001.
[24] L. Mujica, S. Weber, H. Pinto, C. Thomy, F. Vollertsen, Microstructure and mechanical properties of laser-welded joints of TWIP and TRIP steels, Mater. Sci. Eng. A 527 (2010) 2071–2078.
[25] W. Cao, C. Wang, C. Wang, J. Shi, M. Wang, H. Dong, Y. Weng, Microstructures and mechanical properties of the third generation automobile steels fabricated by ART-annealing, Sci. China Technol. Sci. 55 (2012) 1814–1822.
[26] J.-C. Han, S.J. Lee, C.-Y. Lee, S.-J. Lee, S.-Y. Jo, Y.-K. Lee, The size effect of initial martensite constituents on the microstructure and tensile properties of intercritically annealed Fe–9Mn–0.05C steel, Mater. Sci. Eng. A 633 (2015) 9–16.
[27] D.W. Suh, S.J. Park, C.H. Lee, S.J. Kim, Microstructure and mechanical behaviors of 0.1C-13Mn metastable austenitic steel, Metall. Mater. Trans. A Phys. Metall. Mater. Sci. 40 (2009) 264–268.
[28] T. Wang, M. Zhang, W. Xiong, R. Liu, W. Shi, L. Li, Microstructure and tensile properties of the laser welded TWIP steel and the deformation behavior of the fusion zone, Mater. Des. 83 (2015) 103–111.
[29] D.C. Saha, I. Chang, Y.-D. Park, Heat-affected zone liquation crack on resistance spot welded TWIP steels, Mater. Charact. 93 (2014) 40–51.
[30] E. De Moor, D.K. Matlock, J.G. Speera, M.J. Merwin, Austenite stabilization through manganese enrichment, Scr. Mater. 64 (2011) 185–188.
[31] M. Xia, E. Biro, Z. Tian, Y.N. Zhou, Effects of heat input and martensite on HAZ softening in laser welding of dual phase steels, ISIJ Int. 48 (2008) 809–814.
[32] V.H. Baltazar Hernandez, S.S. Nayak, Y. Zhou, Tempering of martensite in dual-phase steels and its effects on softening behavior, Metall. Mater. Trans. A Phys. Metall. Mater. Sci. 42 (2011) 3115–3129.
[33] W. Xu, D. Westerbaan, S.S. Nayak, D.L. Chen, F. Goodwin, Y. Zhou, Tensile and fatigue properties of fiber laser welded high strength low alloy and DP980 dual-phase steel joints, Mater. Des. 43 (2013) 373–383.
[34] J.H. Ryu, D.-I. Kim, H.S. Kim, H.K.D.H. Bhadeshia, D.-W. Suh, Strain partitioning and mechanical stability of retained austenite, Scr. Mater. 63 (2010) 297–299.
[35] J.-H. Ryu, J.-I. Kim, H.-S. Kim, C.-S. Oh, H.K.D.H. Bhadeshia, D.-W. Suh, Austenite stability and heterogeneous deformation in fine-grained transformation-induced plasticity-assisted steel, Scr. Mater. 68 (2013) 933–936.
[36] C.Y. Lee, J. Jeong, J. Han, S.J. Lee, S. Lee, Y.K. Lee, Coupled strengthening in a medium manganese lightweight steel with an inhomogeneously grained structure of austenite, Acta Mater. 84 (2015) 1–8.
[37] S. Lee, B.C. De Cooman, On the selection of the optimal intercritical annealing temperature for medium Mn TRIP steel, Metall. Mater. Trans. A Phys. Metall. Mater. Sci. 44 (2013) 5018–5024.
[38] Y.-K. Lee, B.J. Kwak, J.E. Jin, Microstructures and tensile properties of annealed medium Mn TRIP steels, in: TMS (Ed.), Proc. Conf. PRICM 7, Symposium A, Cairns, Australia 2010, p. 116.